metals

MDPI

Article

Experimental Set-Up of the Production Process and Mechanical Characterization of Metal Foams Manufactured by Lost-PLA Technique with Different Cell Morphology

Girolamo Costanza *, Angelo Del Ferraro and Maria Elisa Tata

Industrial Engineering Department, University of Rome Tor Vergata, 00133 Rome, Italy
* Correspondence: costanza@ing.uniroma2.it; Tel.: +39-06-72597185

Abstract: A flexible and versatile method for manufacturing open-cell metal foams, called lost-PLA, is presented in this work. With a double extruder 3D printer (FDM, Ultimaker S3, Utrecht, The Netherlands), it is possible to make polymer-based samples of the lost model. Through CAD modeling, different geometries were replicated so as to get black PLA samples. This method combines the advantages of rapid prototyping with the possibility of manufacturing Al-alloy specimens with low time to market. The production process is articulated in many steps: PLA foams are inserted into an ultra-resistant plaster mix, after which the polymer is thermally degraded. The next step consists of the gravity casting of the EN-6082 alloy in the plaster form, obtaining metal foams that are interesting from a technological point of view as well as with respect to their mechanical properties. These foam prototypes can find application in the automotive, civil and aeronautical fields due to their high surface/weight ratio, making them optimal for heat exchange and for the ability to absorb energy during compression. The main aspects on which we focus are the set-up of the process parameters and the characterization of the mechanical properties of the manufactured samples. The main production steps are examined at first. After that, the results obtained for mechanical performance during static compression tests with different geometry porosities are compared and discussed. The foam with truncated octahedron cells was found to show the highest absorbed energy/relative density ratio.

Keywords: open cell metal foams; Al alloys; 3D printing; lost PLA

Citation: Costanza, G.; Del Ferraro, A.; Tata, M.E. Experimental Set-Up of the Production Process and Mechanical Characterization of Metal Foams Manufactured by Lost-PLA Technique with Different Cell Morphology. *Metals* **2022**, *12*, 1385. https://doi.org/10.3390/met12081385

Academic Editors: Lovre Krstulović-Opara, Francesca Campana, Michele Bici and Edoardo Mancini

Received: 4 July 2022
Accepted: 15 August 2022
Published: 20 August 2022

1. Introduction

Metal foams are cellular solids composed of a solid and a gas phase. A first classification can be performed on the basis of their porosity: open or closed. The main difference is the presence or absence, respectively, of pore interconnections. The main properties of metal foams are their low density [1–3], high energy absorption in compression [4,5] and crash tests [6,7], high acoustic [8] and vibration [9] absorption, high heat transfer coefficient [10], and high electrical [11] and thermal [12] conductivity. The mechanical behavior is strictly related to the morphology of the porosity [13] and consequently to their production methods [14]. Due to their low density, weight reduction of up to a maximum of 80% can be achieved with respect to the same volume of conventional metals [1,6]. This feature makes them interesting in industrial fields, where lower weights lead to lower fuel consumption, such as in the automotive, aerospace, and naval fields. With respect to mechanical strength, the analysis and comparison must be considered on the basis of weight units, and metal foams demonstrate excellent behavior in compression tests. An interesting feature of open cell foam is its high heat exchange coefficient, thanks to its high surface/volume ratio. One of the most important structural features of metallic foams is their relative density (ρ^*/ρ_o), which is the ratio of the density of the foam to the density of the solid. In general, metal foams can easily reach relative densities lower than 0.3. Gibson and Ashby [15] analyzed the properties of cellular materials with respect to the way in which the solid was distributed in the cell faces and edges. They described the topological laws governing the

shape and size of the cells, and then the equations describing the relationship between the density and the cell wall thickness and length were developed for cellular solids. Below, the formulas for the correlation between relative density and different type of cells are reported for three-dimensional open cells (aspect ratio Ar = h/l). The relationship between relative density and mechanical properties has also been studied by Gibson and Ashby [15], Bin et al. [16], and Jing et al. [17]. Another feature of metal foams is their ability to absorb energy during compression, and a typical graph (stress–strain), displayed in Figure 1 [4], indicates a starting step exhibiting pseudoelastic behavior, a second plateau step in which the average stress remains constant and the cavities begin to collapse, followed by a third step in which foam densification leads to a rapid increase in stress. On the basis of an analysis of the area under the curve, it can be observed that cellular materials are capable of high energy absorption, both for static and for dynamic loads.

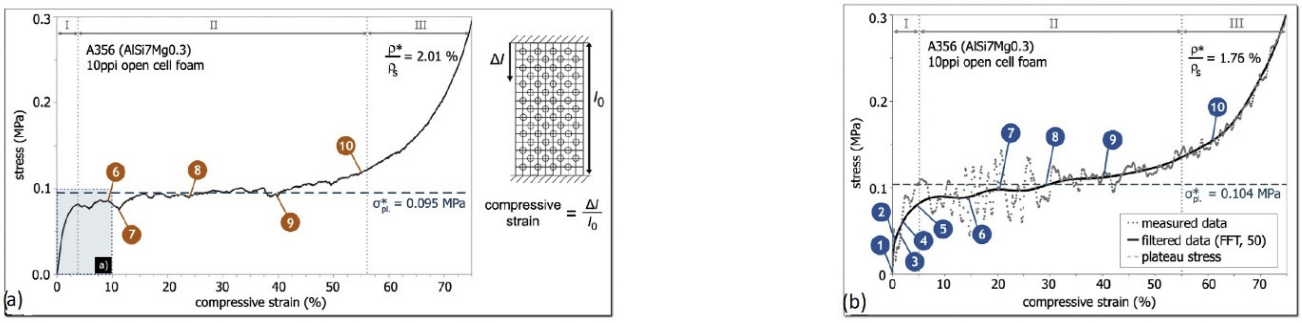

Figure 1. (**a**) σ-ε curve for static load. (**b**) σ-ε curve for dynamic load (1000 mm/s speed) in an Al-Si truncated octahedron structure [4].

From a technological point of view, different production processes give rise to different shape porosities and, consequently, different properties [18], as well as different fields of application. The processing of open-pore metal foams mainly employs sintering or casting techniques [19]. The method used in this study is "the lost PLA" with the polymer preform. This method comprises a number of different steps: CAD modeling of the open-pore foam, 3D printing of the model using PLA, plaster casting on the PLA model, mold drying, removal of PLA from the plaster, metal casting in the plaster mold (700 °C), plaster removal, and, finally, wash cleaning. The flexibility of this method allows the preselection of shaped pores in accordance with the intended final application, with periodic metallic cellular lattices as described in [20,21], using the fused filament technique and on the basis of morphological characterization. Richard and Kwok [22] compared the mechanical properties, but in a manner limited to the onset of plastic deformation, while Nicolas et al. [23] only examined up to a displacement of 12 mm. Snelling et al. [24] used the finite element method to analyze the energy absorption capability compared to a solid block of the same weight. Finally, in [25], Umanzor et al. experimentally and computationally studied the impact resistance of a target per unit area of mass of an A356 alloy–ceramic lattice structure with ceramic tiles encapsulated in the metal matrix. In this paper, the different geometrical features and the consequent compressive behavior of the manufactured foams up until the point of final densification are described and discussed.

2. Materials and Methods

Al 6082 alloy was the base material selected for the manufacturing of the foams using the modified investment casting technique. The production process was inspired by an ancient technique called "lost wax". Specifically, in this method, a wax model was created and covered with a clay mold with holes that would allow the wax to come out. When subjected to heating, the clay would become terracotta, and the wax model would come out of the cavities, forming the negative shape of the object, which would subsequently be used to cast the bronze. The process consists of the following main steps: build-up the model

using 3D CAD; export to CAM software (Ultimaker Cura 3.0, Utrecht, The Netherlands) for 3D printing; 3D print the model using PLA; plaster cast the PLA model; mold drying; removal of PLA from the plaster; cast the metal in the plaster mold; remove the plaster to obtain the foam. A scheme of the process is showed in Figure 2.

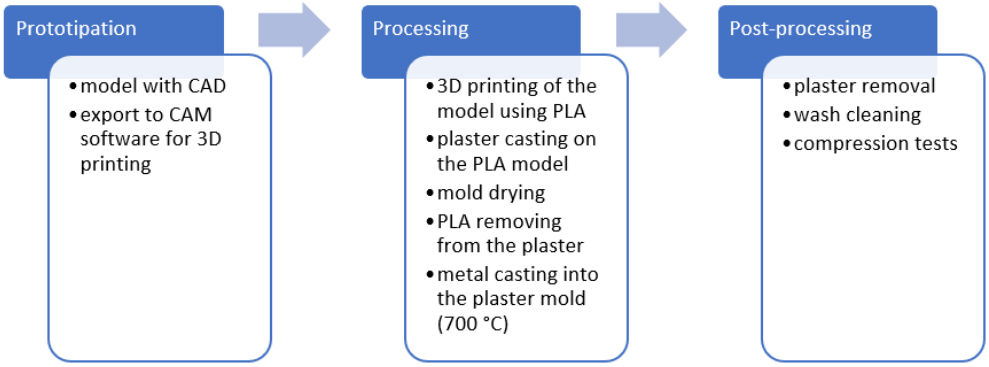

Figure 2. Scheme of the production process.

The main advantage of adopting such a method is the possibility of preselecting the size and shape of the pores in the final foam, as a function of the final application and in line with the required performance, using a technique that offers low cost and good repeatability. Specifically, CAD models were developed starting from the geometries shown in Figure 3, stacking them in order to maintain symmetry and to optimize the filling of the space. Geometries with increasing degrees of complexity were chosen in order to test the dependence of the performance on changes in shape. In Figure 4, renderings of the models printed in the laboratory are presented; the printed PLA foams are presented in Figure 5.

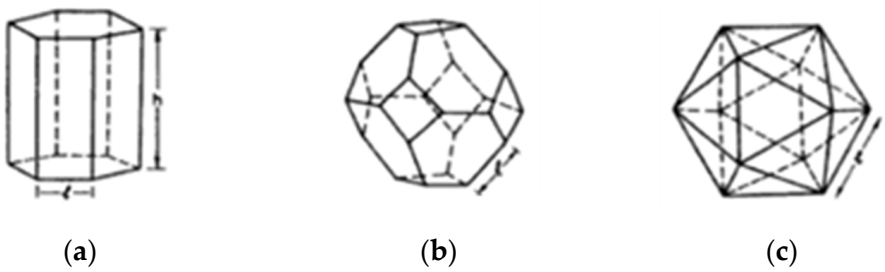

Figure 3. (**a**) Hexagonal with rectangular cell; (**b**) Truncated octahedron; (**c**) Icosahedron.

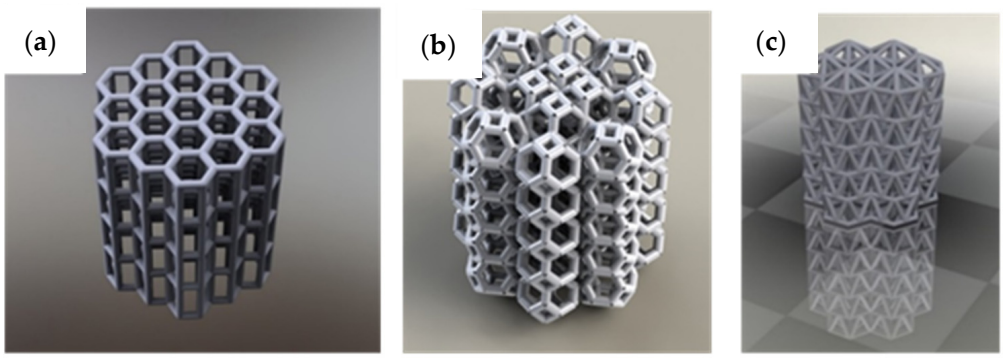

Figure 4. Renderings of CAD models: (**a**) hexagonal with rectangular cell; (**b**) truncated octahedron; (**c**) icosahedron.

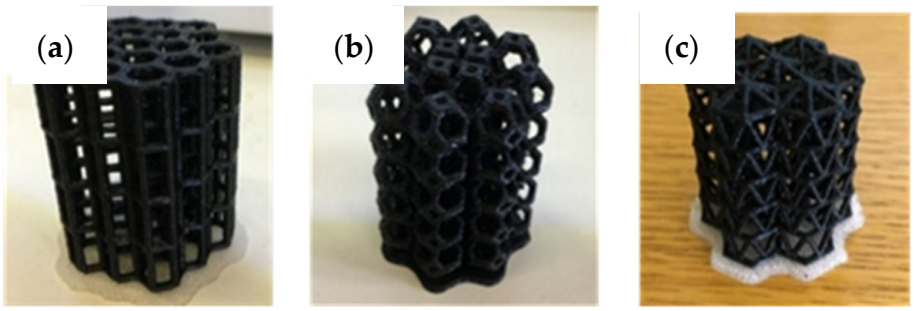

Figure 5. Printed PLA foams: (**a**) hexagonal with rectangular cell; (**b**) truncated octahedron; (**c**) icosahedron.

After creating the CAD model and generating the STL file for the 3D Ultimaker S3 printer, the model was printed using black PLA. The printing process also required the parameters to be defined (printing speed = 45–60 mm/s; layer height = 0.3–1.0 mm, initial layer height 0.15–0.50 mm, support generation and lower base in natural PVA). The number of layers is a function of the layer height parameter, which was chosen as a compromise between the time required for printing and the desired precision of the PLA model, in such a way as to avoid the defect known as "shifted layer". Moreover, the use of a PVA base insertion allows the simpler removal of some parts, because it is water soluble, without the risk of damaging the prototype. As a result, there was a lower mass of polymer needing to be removed from the mold. After printing, the PLA model was placed into an AISI 316 mold. The mold was built up by pouring a mixture of dental plaster and water (3:1) over the PLA model, which was subsequently allowed to dry in air for 15–20 min and then placed in an oven at 750 °C to degrade the polymer. Three types of plaster were used: alabaster plaster, type 4 dental plaster, and plaster of Paris. Once the polymer was eliminated, the Al alloy was poured using gravity to build the final foam model. EN 6082 (AlSi1MgMn) alloy was used for casting. In a final step, the samples were cleaned by water jet to remove any residual investment. The different steps of the foam production process are illustrated in Figure 6.

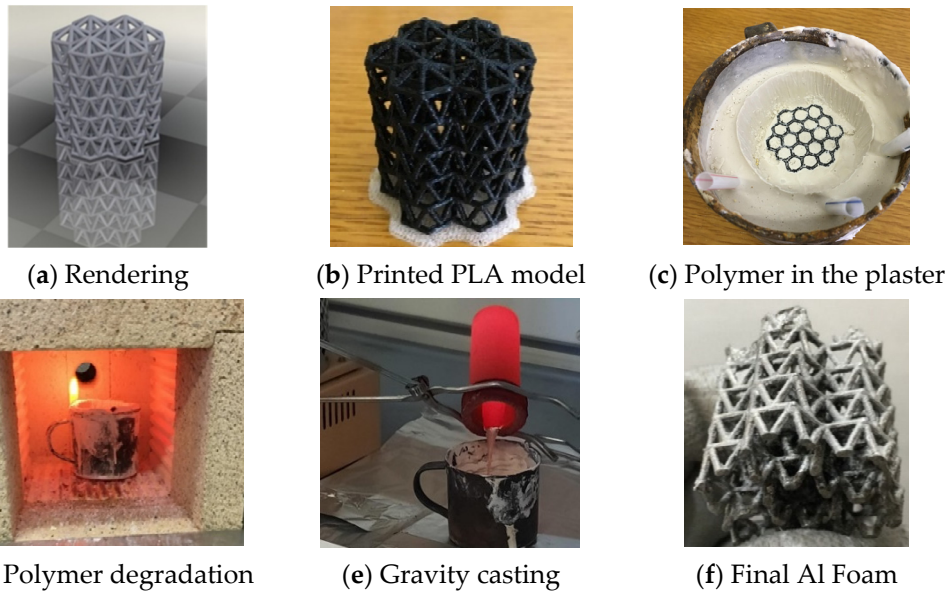

(**a**) Rendering (**b**) Printed PLA model (**c**) Polymer in the plaster

(**d**) Polymer degradation (**e**) Gravity casting (**f**) Final Al Foam

Figure 6. The six steps of the foam manufacturing process: (**a**) rendering of the model; (**b**) printing of the model; (**c**) polymer in the plaster; (**d**) polymer degradation; (**e**) gravity casting; (**f**) final Al foam.

3. Experimental Results

The obtained polymer models were analyzed using a stereo microscope in order to detect any defects and their correlation with the selected printing parameters. In Figure 7a, a layer detachment is shown. The filament was probably subjected to localized stresses that led to an irregular geometry during deposition. In Figure 7b, "stringing" is evident, which consists of thin wire like a spider's web as over-extrusion. The latter defects are due to the lack of underlying material. Layers and mass that are too large lead to expansion while the underlying material tends to cool down suddenly, damaging the macrostructure. On the basis of experimentation (decreasing the layer height, the initial layer height, and the temperature), a significant improvement was achieved: detachment of the layers is no longer present, as can be seen in Figure 7c. Adherence is therefore complete; however, by further decreasing the layer thickness, the accuracy increases. This result shows the optimal choice between two opposite effects: the quality of the surface finish and production time. The slight stringing present should also be noted; however, this does not affect the precision of the plaster mold or the subsequent casting.

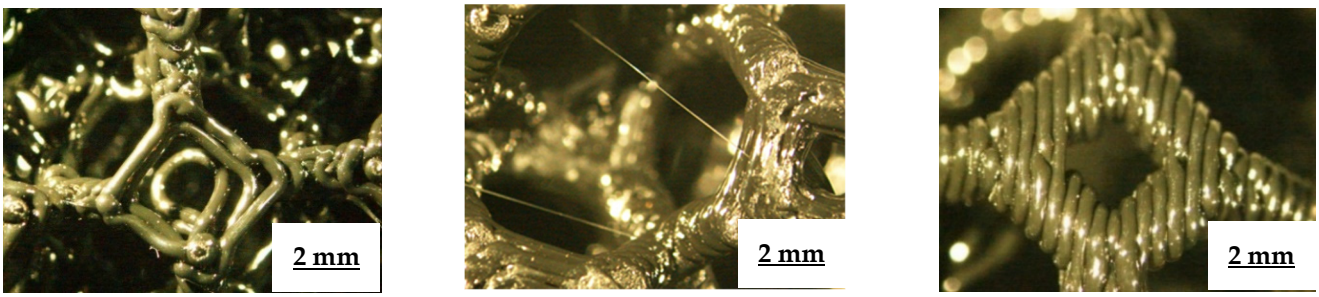

(**a**) Square cell (**b**) Square cell (**c**) Hexagonal cell

Figure 7. Stereo microscope images (10×). (**a**) Layer detachment. (**b**) Stringing. (**c**) Absence of defects after the definition of the printing parameters.

Experiments were also carried out with respect to the plaster; in particular, it was found that by mixing type 4 dental plaster and alabaster plaster, easier removal of the plaster from the final foam could be achieved. A defect arising from the incorrect plaster mix is shown in Figure 8a: when only plaster of Paris was used, a clear infiltration of Al alloy into the mold was detected. The best results were achieved by increasing the amount of dental type 4 plaster to 70%, with 30% alabaster plaster. In this way, the optimal results in terms of casting and plaster removal were achieved.

Several aspects of casting were revealed to be critical, as well. The most important were the following: melting temperature, conditioning time of Al alloy in the oven, and casting time, which impacts the viscosity of the melt and the formation of Al_2O_3, hindering the casting itself. The best results were achieved with an oven temperature of 750 °C. To obtain a suitable evacuation of gases, three vents were adopted in the plaster mold. The completely formed cellular structure, with only three hexagons that are not crossed by molten metal, can be observed in Figure 8b,c. The major defect at this stage was that in the junction between the model and the vent channel, with Al infiltration of alloys being evidenced. A solution was found by providing a lower support for the foams that had already been printed where the vent channels were joined. Another problem encountered was as a result of the Al alloy melting in the vent channels and on the sprue. This problem resulted in the incomplete geometry of the model near the channel (Figure 8b). To avoid this defect, a greater amount of plaster was used, leading to the complete filling of the steel cup in order to obtain a greater difference in level between the vent channels and the casting connection. This made it possible for the molten metal to remain in the sprue. Another critical aspect was the identification of the mix of the plaster. In Figure 8a, an example of infiltration of Al alloy into the elementary cells due to the collapse of the plaster in that region is shown. The mix "plaster of Paris" demonstrated properties that were far

removed from the optimal ones, which were achievable only when using dental plaster type 4. In this case, in addition to mold embrittlement, another problem occurred that was related to the strong expansion undergone by the gypsum during heating. The amount of water is a very sensitive parameter in the mixture. Smaller amounts of water create a different effect, whereby the compound is too dense, and is therefore unable to infiltrate the polymer model. For this reason, it was decided to increase the amount of dental plaster type 4 with respect to the alabaster plaster. Subsequently, two castings were performed, using 30% and 40% alabaster plaster, respectively, with dental plaster type 4 accounting for the remainder. This led to the best results in terms of casting and mold removal. The results obtained in the gravity casting experiments were analyzed using a stereo microscope, and the main defects (porosities) were observed, as shown in Figure 8d,e, as well as the layers, as shown in Figure 8f. It should be noted that the layer structure does not negatively affect the compression mechanical properties, and for this reason, no investigation was performed. In Figure 9, the same microstructure is highlighted due to the quality of the mold created using type 4 dental plaster, which faithfully maintained the geometry created in the black PLA.

(**a**) Infiltration of Al alloy into the mold.

(**b**) Cells not completed at the border.

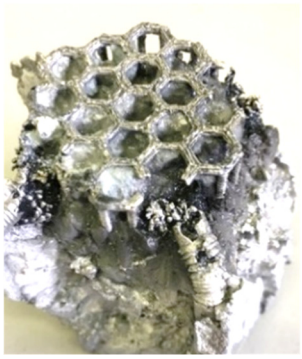

(**c**) Infiltration of Al into the vents.

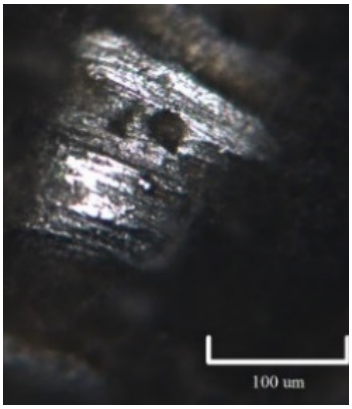

(**d**) Porosity of the hexagonal cell foam, 100× optical microscopy.

(**e**) Porosity of the foam, 100× optical microscopy.

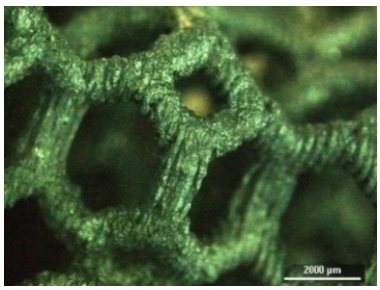

(**f**) Truncated octahedron elementary cell of Al alloy foam, layer evidenced.

Figure 8. Main defects in Al alloy open foam. (**a**) Al infiltration; (**b**) cells not completed; (**c**) infiltration of Al in the vents; (**d**,**e**) porosity of hexagonal cell foam; (**f**) layer evidenced in truncated octahedron elementary cell Al alloy foam.

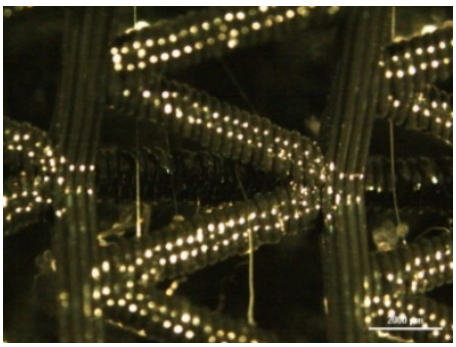

(**a**) Black PLA foam.

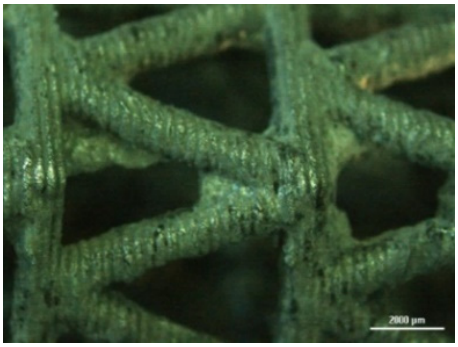

(**b**) Al alloy foam.

Figure 9. Stereo microscope observations: (**a**) black PLA foam; (**b**) Al alloy foam.

After manufacturing, the foam samples underwent compression tests at a constant crosshead speed (5 mm/min). The main results are reported in Figure 10, while the most important parameters are summarized in Table 1, where the geometrical properties and adsorbed energies are reported. In the table, the theoretical area is obtained in consideration of the edge of the foam (top view): the effective area is the average difference between the minimum and maximum area (Table 2). The specific energy was always calculated relative to the effective resistant area. All the foams exhibited a final densification, and as such, the area under the curve was considered in order to calculate the effective specific absorbed energy (Figure 11).

(**a**) Icosahedron

(**b**) Hexagonal 3

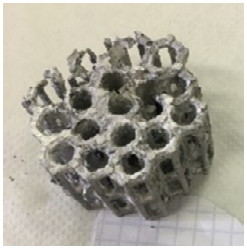

(**c**) Hexagonal 5

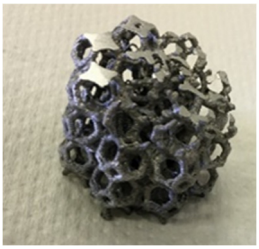

(**d**) Truncated octahedron

Figure 10. Al open cell manufactured foams: (**a**) icosahedral; (**b**) hexagonal; (**c**) hexagonal; (**d**) truncated octahedral.

Table 1. Geometrical data and properties of manufactured foams.

	Height (mm)	**Theoretical Area (mm^2)**	**Effective Area (mm^2)**	**Effective Specific Energy at σ = 109 MPa (MJ/m^3)**
Sample 1: Icosahedral cell	36.3	909.8	185.5	17
Sample 2: Hexagonal cell	32	895.5	253.7	26.2
Sample 3: Hexagonal cell	21.5	895.5	253.7	19.3
Sample 4: Truncated octahedral cell	25.5	854.4	279.3	23.4

Table 2. Minimum and maximum area.

Area Min	Area Max
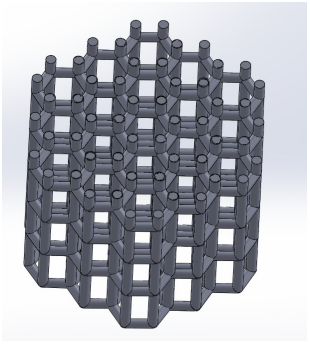	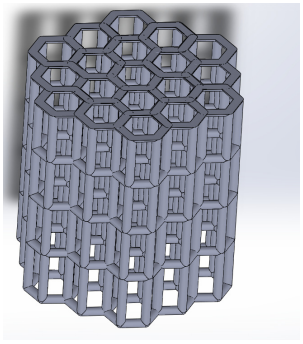

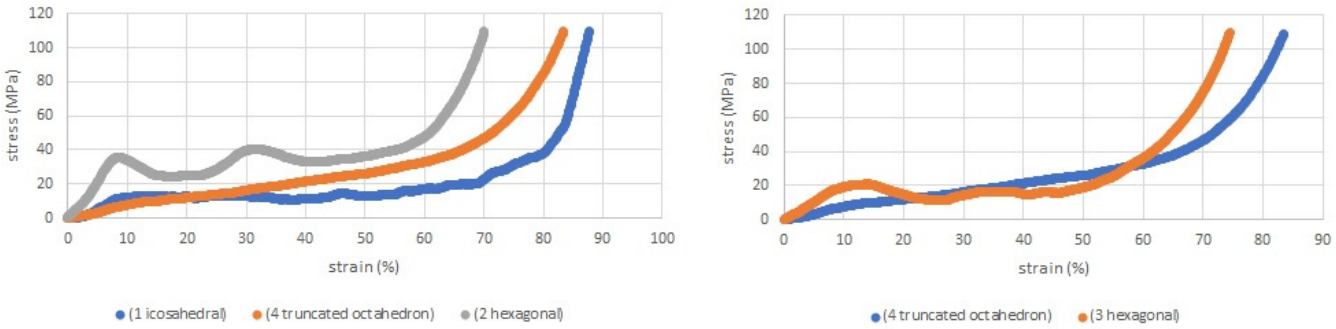

Figure 11. Stress–strain curves for icosahedral (1), hexagonal (2), hexagonal (3) and truncated octahedron (4).

Sample 2, with hexagonal cells, exhibited an absorbed energy of 26.2 MJ/m^3, while Sample 4, with truncated octahedral cells, exhibited an absorbed energy of 23.4 MJ/m^3. Despite this small difference, the hexagonal cell foam (Sample 2) exhibited the maximum value of absorbed energy. Furthermore, this foam showed localized instabilities; for this reason it was subjected to local stress decrease (twice) in the compression curve. The results regarding absorbed energy at the same maximum stress (σ = 109 MPa) were compared for Samples 3 and 4. This value of stress was chosen in order to be able to perform comparisons under the same applied stress, but without penalizing geometries that showed a lower load level. Sample 3 had a height of 21.5 mm, and one cell stack less than Sample 2. In the comparison, the truncated octahedral cell foam's behavior was better than the hexagonal cell (Sample 2). The absorbed energy was strictly correlated with the height, and a comparison between different geometries could be performed by using the same height. To do this, linear interpolation was used to obtain an estimation of the absorbed energy for the hexagonal cell at 25.5 mm, i.e., the height of Sample 4. This technique is effective due to the nonlinearity of the curves, thus giving a value very close to the real one.

On the hexagonal Samples 2 and 3, with heights of 32 and 21.5 mm, respectively, the linear interpolation of the specific absorbed energy was carried out as a function of height. By adopting the linear interpolation formula, it was possible to extrapolate the absorbed energy at a height corresponding to the hexagonal cell (25.5 mm).

$$\frac{25.5 - 21.5}{32 - 21.5} = \frac{x - 19.3}{26.2 - 19.3} \qquad x = 21.9 \text{ MJ/m}^3 \tag{1}$$

4. Discussion

Formula (1) demonstrates that the truncated octahedron cells are capable of absorbing a greater amount of energy than the hexagonal foam, with a more uniform stress distribution.

Such a structure, thanks to the greater surface/volume ratio, shows a more distributed stress trend fluctuation. Even for the foam with icosahedral cells, homogeneous plasticization without fluctuations in terms of load was noted. This aspect is related to the overall deformation of the sample, which tends to plasticize in a uniform fashion. Conversely, in the samples with hexagonal cells, the onset of localized instabilities was observed, causing the typical bending of the curve due to the load fluctuations. The exact point at which the load increased was at the transition between the failure caused by the first instability and the second buckling of the lower stack to go down again after deformation. However, it should be noted that, in the case of dynamic load, the onset of localized deformations is an advantage in some applications, because it guarantees a more accurate prediction of behavior under high degrees of deformation, making it possible to identify the starting point of failure. On the basis of the tests carried out, it can be observed that, under the same normal load, the samples deform differently as the geometry of the cell changes. When the specimens were subjected to combined loads, and shear and normal stress, the deformation behavior underwent other variations. This highlights the fact that the optimal geometry must be selected during the design phase on the basis of the variations in load conditions in order to obtain the most efficient performance.

Another aspect to be highlighted is the possibility of recreating models with attention to detail. The microscopic analysis of Al alloy foams shows that they have the same layers as the PLA samples. This aspect guarantees high versatility, making it appropriate for use in sectors where aesthetics is a very important factor. For instance, it is possible to manufacture jewels or statues with very complex shapes, giving this technology a relevant place in the art and goldsmithing sector. The production process for the lost-PLA technique implies many potential applications and a variety of different paths arising from the market need to create new objects in relatively short periods of time in order to be competitive on the market. The manufacturing of different geometries makes it possible to compare the energy absorption performance of hexagonal cell foam and truncated octahedron cell. Relative density can be measured as a function of the following geometrical parameters: "t" cell thickness, "l" cell side, and ρ/ρ_s relative density. The results are summarized in Table 3. The best performance in terms of density and specific energy was achieved by the truncated octahedron cell. It is also important to consider the average plateau stress for both foams, the values of which were comparable at about 20 MPa.

Table 3. Comparison of geometrical properties, relative density, and energy absorption for the two best performing manufactured foams.

	t (mm)	l (mm)	ρ/ρ_s	Specific Energy at 109 MPa	Real Volume (m^3)	Absorbed Energy (MJ) at 109 MPa
Hexagonal cell sample (height 25.5 mm)	1.5	4	0.17	21.9	6.4×10^{-6}	0.35
truncated octahedron cell sample (height 25.5 mm)	1.57	2.94	0.30	23.4	7.1×10^{-6}	0.41

5. Conclusions

In this work, the steps of the production process of open-cell foams using the lost-PLA technique were demonstrated, focusing on the critical issues in the various steps. This technique exhibits all of the advantages of rapid prototyping, i.e., the possibility of obtaining metal foams in a short time. Following a series of experiments, it was possible to obtain first samples with acceptable results in terms of morphology, surface finish, and mechanical properties. At the end of this stage, the printing parameters, plaster mix, melting temperature and time, and casting time were identified. It was possible to obtain an Al alloy open cell foam in only six hours. These manufactured foams possessed the same surface features as the PLA foams manufactured using a 3D printer. Another advantage is the possibility of obtaining functional samples that are useful in a number of industrial

fields. This process consists of easy steps and makes it possible to obtain CAD models with a high variety of geometries and a reduced time to market. However, there are still some open problems that remain to be solved; for example, with respect to the porosity resulting from gravity casting. Such defects cause a reduction in performance not present when using the standard casting process. Another problem is related to the production costs, because the crucible tends to wear out after a short time. Furthermore, type 4 dental plaster is more expensive than alabaster plaster, so it is not the cheapest technique for manufacturing large quantities of the same sample. The proposed process, however, is optimal for the production of physical prototypes in the testing phase that can be used as a design aid. This reflects the design philosophy for manufacturing, where an interconnection is created between design and production. It also solves the problem inherent in other processes, where the success of highly complex geometries is not guaranteed, thus giving freedom to the designer. Prototypes were also manufactured that demonstrated high energy absorption during compression tests. One limitation is the size of the foam, which is dictated by the print volume of the FDM machine. It should be noted that experiments with metal foams, which are widely used in special applications (in the automotive, civil, aerospace and aeronautics industries), have been performed. This has been demonstrated to be an efficient process in terms of the models obtained and their surface finish. This was unthinkable in the past, when prototypes, made of either wood or wax, had physical properties so far removed from the finished prototype. In summary, open cell metal foams were manufactured as conceived and designed in a way that was cheap, and offered good repeatability and mechanical performance in terms of absorbed energy under compression tests.

Author Contributions: All the authors contributed equally to the different steps: conceptualization, methodology, software, formal analysis, investigation, resources, data curation, writing, review, and editing. All authors have read and agreed to the published version of the manuscript.

Funding: This research received no external funding.

Institutional Review Board Statement: Not applicable.

Informed Consent Statement: Not applicable.

Data Availability Statement: Not applicable.

Acknowledgments: The authors are grateful to Piero Plini and Benedetto Iacovone for technical support in the experiments.

Conflicts of Interest: The authors declare no conflict of interest.

References

1. Banhart, J. Manufacture, characterization and application of cellular metals and metal foams. *Prog. Mater. Sci.* **2001**, *46*, 559–632. [CrossRef]
2. Brugnolo, F.; Costanza, G.; Tata, M.E. Manufacturing and characterization of AlSi Foams as core materials. *Proc. Eng.* **2015**, *109*, 219–227. [CrossRef]
3. Costanza, G.; Tata, M.E.; Trillicoso, G. Al foams manufactured by PLA replication and sacrifice. *Int. J. Lightweight Mater. Manuf.* **2021**, *4*, 62–66. [CrossRef]
4. Schuler, P.; Fischer, S.F.; Buhrig-Polaczek, A.; Fleck, C. Deformation and failure behaviour of open cell Al foams under quasistatic and impact loading. *Mater. Sci. Eng. A* **2013**, *587*, 250–261. [CrossRef]
5. Zhou, J.; Shrotriya, P.; Soboyejo, W.O. Mechanisms and mechanics of compressive deformation in open-cell Al foams. *Mech. Mater.* **2004**, *36*, 781–797. [CrossRef]
6. Song, H.W.; Fan, Z.J.; Yu, G.; Wang, Q.C.; Tobota, A. Partition energy absorption of axially crushed aluminum foam-filled hat sections. *Int. J. Sol. Struct.* **2005**, *42*, 2575–2600. [CrossRef]
7. Costanza, G.; Tata, M.E. Dynamic and static compressive behaviour of aluminium foam. In Proceedings of the 4th International Structural Engineering and Construction, Melbourne, Australia, 25 September 2007.
8. Hinze, B.; Rosler, J. Measuring and simulating acoustic absorption of open-celled metals. *Adv. Eng. Mater.* **2014**, *16*, 284–288. [CrossRef]
9. Albertelli, P.; Esposito, S.; Mussi, V.; Goletti, M.; Monno, M. Effect of metal foam on vibration damping and its modelling. *Int. J. Adv. Manuf. Technol.* **2021**, *117*, 2349–2358. [CrossRef]

10. Guarino, S.; Barbieri, M.; Pasqualino, P.; Bella, G. Fabrication and characterization of an innovative heat exchanger with open cell aluminum foams. *Energy Proc.* **2017**, *118*, 227–232. [CrossRef]
11. Dharmasena, K.P.; Wadley, H.N.G. Electrical conductivity of open-cell metal foams. *J. Mater. Res.* **2002**, *17*, 625–631. [CrossRef]
12. Matz, A.M.; Mocker, B.S.; Jost, N.; Krug, P. Effective thermal conductivity of open-pore metal foams as a function of the base material. *Mater. Test.* **2015**, *57*, 825–836. [CrossRef]
13. Costanza, G.; Giudice, F.; Sili, A.; Tata, M.E. Correlation modeling between morphology and compression behavior of closed-cell Al foams based on X-ray computed tomography observations. *Metals* **2021**, *11*, 1370. [CrossRef]
14. Costanza, G.; Tata, M.E. Mechanical behavior of PCMT and SDP Al foams: A comparison. *Proc. Struct. Int.* **2020**, *25*, 55–62. [CrossRef]
15. Gibson, L.J.; Ashby, M.F. *Cellular Solids. Structure and Properties*, 2nd ed.; Cambridge University Press: Cambridge, UK, 1997.
16. Bin, J.; Zejun, W.; Naiqin, Z. Effect of pore size and relative density on the mechanical properties of open cell aluminum foams. *Scr. Mater.* **2007**, *56*, 169–172.
17. Jing, L.; Su, X.; Yang, F.; Ma, H.; Zhao, L. Compressive strain rate dependence and constitutive modeling of closed-cell aluminum foams with various relative densities. *J. Mater. Sci.* **2018**, *53*, 14739–14757. [CrossRef]
18. Ashby, M.F.; Medalist, R.F.M. The mechanical properties of cellular solids. *Metall. Trans. A* **1983**, *14*, 1755–1769. [CrossRef]
19. Wadley, H.N. Cellular metals manufacturing. *Adv. Eng. Mater.* **2002**, *4*, 726–733. [CrossRef]
20. Carneiro, V.H.; Rawson, S.D.; Puga, H.; Meireles, J.; Withers, P.J. Additive manufacturing assisted investment casting: A low-cost method to fabricate periodic metallic cellular lattices. *Addit. Manuf.* **2020**, *33*, 101085. [CrossRef]
21. Carneiro, V.H.; Rawson, S.D.; Puga, H.; Withers, P.J. Macro-, meso-and microstructural characterization of metallic lattice structures manufactured by additive manufacturing assisted investment casting. *Sci. Rep.* **2021**, *11*, 4974. [CrossRef]
22. Richard, C.T.; Kwok, T.H. Analysis and Design of Lattice Structures for Rapid-Investment Casting. *Materials* **2021**, *14*, 4867. [CrossRef]
23. Meisel, N.A.; Williams, C.B.; Druschitz, A. Lightweight metal cellular structures via indirect 3D printing and casting. In Proceedings of the 2012 International Solid Freeform Fabrication Symposium, University of Texas at Austin, Austin, TX, USA, 6–8 August 2012.
24. Snelling, D.; Li, Q.; Meisel, N.; Williams, C.B.; Batra, R.C.; Druschitz, A.P. Lightweight metal cellular structures fabricated via 3D printing of sand cast molds. *Adv. Eng. Mater.* **2015**, *17*, 923–932. [CrossRef]
25. Umanzor, M.E.; Batra, R.C.; Williams, C.B.; Druschitz, A.P. Penetration Resistance of Cast Metal− Ceramic Composite Lattice Structures. *Adv. Eng. Mater.* **2021**, *23*, 2100577. [CrossRef]